Inorganic Chemistry

Article

pubs.acs.org/IC

Electronic and Magnetic Structures of Hole Doped Trilayer $La_{4-x}Sr_xNi_3O_8$ from First-Principles Calculations

Lokanath Patra,[†] M. R. Ashwin Kishore,[†] Ravindran Vidya,[‡] Anja O. Sjåstad,[¶] Helmer Fjellvåg,[¶] and Ponniah Ravindran*,[†,¶]

[†]Department of Physics, Central University of Tamil Nadu, Thiruvarur 610101, India

[‡]Department of Medical Physics, Anna University, Chennai 600025, India

[¶]Center for Materials Science and Nanotechnology and Department of Chemistry, University of Oslo, Box 1033 Blindern, N-0315 Oslo, Norway

ABSTRACT: The magnetic and electronic properties of trilayer $La_4Ni_3O_8$, similar to hole-doped cuprates, are investigated by performing full-potential linearized augmented plane wave method-based spin-polarized calculations with LDA and GGA functionals including Hubbard U parameters to account for strong correlation effects. On the basis of these calculations, we found that $La_4Ni_3O_8$ is a C-type anti-ferromagnetic (C-AFM) Mott insulator in agreement with previous experimental and theoretical observations. Our calculations suggest that the two crystallographically nonequivalent nickel atoms Ni1 and Ni2 are found to be in high-spin state with an average valency of +1.33. Intermediate band-gap states are originated from d_{z^2} electrons of both types of Ni ions after including the strong correlation effects. To understand the role of hole doping on electronic structure, phase stability, and magnetic properties of $La_4Ni_3O_8$, similar calculations were performed for $La_{4-x}Sr_xNi_3O_8$ as a function of x, using the supercell approach. We found that the hole doping brings insulator-to-metal transition without changing the C-AFM ordering, though the magnetic moment is enhanced at both Ni sites. Moreover, these Ni atoms are always in an average valence state irrespective of hole doping or volume change. So the electronic properties of hole-doped $La_4Ni_3O_8$ cannot be compared with hole-doped cuprates that are high-T_C superconductors.

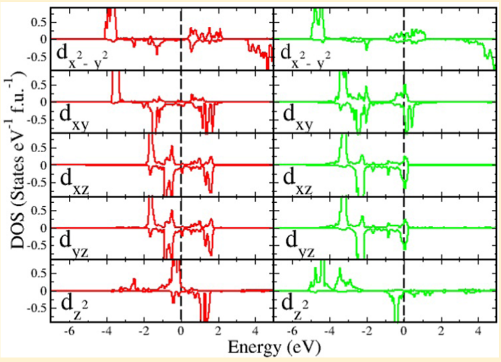

INTRODUCTION

The discovery of superconductivity in cuprates[1] has aroused extended interest in this fascinating phenomenon in other transition-metal oxides, especially in neighboring nickelates. Nickelates have the potential to exhibit physics similar to high-T_C cuprates[2−4] because the electronic configuration of constituent Ni^+ ($3d^9$) is equal to Cu^{2+} in the high-T_C cuprates. Since these compounds appear to have electrons rather than holes as charge carriers, there has been considerable interest in the electronic properties of these materials. Furthermore, theoretical studies[2] suggest that only nickelates with Ni^+ ($3d^9$, $S = \frac{1}{2}$) can form an anti-ferromagnetic (AFM) insulator that can be doped with Ni^{2+} holes similar to hole-doped superconducting cuprates.

The nickelate $La_4Ni_3O_8$, discovered in the late 1990s, contains Ni ions in a square-planar coordination and has become a focus of interest. It is a member of the so-called T′-type $Ln_{n+1}Ni_nO_{2n+2}$ (Ln = La, Nd; n = 2, 3, and ∞) homologous series, which can be prepared by intermediate-temperature reduction of the Ruddlesden−Popper (RP) $Ln_{n+1}Ni_nO_{3n+1}$.[3] La−Ni−O system was initially investigated by Bednorz and Müller for the possibility of superconductivity with Ni in 2+ and 3+ oxidation states.[5] Their discovery stimulated the research interest to look for superconductivity in other transition-metal oxides with low-dimensional crystal structures like cuprates, which are favorable for superconductivity. Nickel in 1+ state in square-planar coordination can be very similar to the high-T_C cuprates, but Ni with 1+ oxidation state was difficult to stabilize at that time. Anisimov et al.[2] predicted theoretically that nickelates having the mixed valence of Ni^+/Ni^{2+} have electronic configuration similar to the hole-doped superconducting cuprates Cu^{2+}/Cu^{3+}, which show high temperature superconductivity.

At low temperatures the La−Ni−O system undergoes metal-to-insulator transition[6] as a function of its thickness. This happens due to electron correlation, band effect, and also by spin, orbital, and charge ordering.[7−9] Pardo et al.[10] anticipated that the pressure-induced metal-to-insulator transition takes place at 0 K, and high-spin state to low-spin state transition occurs at 105 K. Also $La_4Ni_3O_8$ can either be in ferromagnetic (FM)−metallic low-spin (LS) phase or an anti-ferromagnetic−insulating high-spin (HS) phase. Dimensionality-induced insulator-to-metal transition was reported by Liu et al.[7] in $La_{n+1}Ni_nO_{2n+2}$ system, as its dimensionality changes with variation with n (n = 2, 3, and ∞). The magnetic properties of this material series are determined by the spin states of Ni^+

Received: August 18, 2016
Published: November 3, 2016

DOI: 10.1021/acs.inorgchem.6b01938
Inorg. Chem. 2016, 55, 11898−11907

and Ni^{2+}. Correspondingly, Poltavets et al.[11] and N ApRoberts-Warren et al.[12] have shown from nuclear magnetic resonance (NMR) measurements that $La_4Ni_3O_8$ undergoes an AFM transition at T_N = 105 K. Pardo et al.[10,13] and Liu et al.[14] also reported that $La_4Ni_3O_8$ is AFM with *C*-AFM ordering in the ground state, which is a molecular correlated insulator. Moreover, they have reported that the insulating state is originating from strong interlayer coupling and electronic correlation effects.

Using the muffin-tin orbital (MTO) based linear MTO (LMTO) and *N*th-order MTO (NMTO)[15,16] methods, Sarkar et al.[17] showed that $La_4Ni_3O_8$ in the *A*-AFM and FM ordering possess Ni in low-spin state and correlated metallic ground state, which is against the experimental observations.[11] Recently, the electrical resistivity of $La_4Ni_3O_8$ has been measured under pressure, and a suppression of the high-spin state was observed.[18] Nevertheless, neither metallic state nor superconductivity has been seen under pressure (~50 GPa), and this may be due to the displacement of the oxygen atoms at high pressures. Among various scarcely metallic 3d electron systems, hole-doped nickel oxides with K_2NiF_4 type of structure, for example, $(La,Sr)_2NiO_4$, are found to prompt metallic conductivity, yet more gradually than in the cuprates.[19] Essentially more Sr substitution is important to prompt metallic-type conductivities; that is, the $La_{2-x}Sr_xNiO_4$ system shows low-temperature conductivity for x close to 1. Doping at *A* site by a suitable ion is one of the tools that could induce tremendous variation in the electrical and magnetic behavior of these RP phases. Chokkha et al.[20] have reported that Sr doping at La site reduces the electrical conductivity of $La_4Ni_3O_{10\pm\delta}$ and further decreases with an increasing amount of Sr. The insulating La_2CuO_4 transforms to superconducting[21] state when it is doped with holes; that is, some of the lanthanum atoms are replaced by bivalent alkaline earth ion or basic monovalent cation with suitable ionic size. Enthalpy of formation of $La_{2-x}A_xCuO_4$ (A = Ba, Sr, Ca, and Pb) indicates that more basic *A*-site cations tend to energetically balance out higher oxidation states of *B*-site cations, which is responsible for the change in electrical properties in the parent material.[22] To observe the change in properties as a function of doping at *A*-site, $La_{2-x}Sr_xNiO_4$ is another interesting system to study. This material behaves like an AFM-insulator for $x = 0$. For the higher Sr substitution range, that is, $0.5 \leq x \leq 0.9$, $La_{2-x}Sr_xNiO_4$ behaves like a nonmetal and shows the electrical conduction with variable ranges of hopping mechanism at low temperature and exponentially activated conduction at comparatively higher temperatures. The metallic conductivity sets in for concentration of x ranging from 1.0 and 1.3. Resistivity data in the temperature range up to 25 K follows $T^{1/2}$ dependence for the x value beyond 1.3, where strong electron−electron interactions occur in the presence of disorder in a diffusive metallic phase.[23] Orthorhombic $Nd_2NiO_{4\pm\delta}$ undergoes a phase transition to pseudo-tetragonal symmetry upon substitution with Sr^{2+} at Nd site.[24] The increased magnetic moment in the $Nd_{2-x}Sr_xNiO_4$ system with increase in x is attributed to the frustration of AF pairing that originates from the mixed valence of Ni^{2+}/Ni^{3+}, while it showed a metal-semiconductor transition that is related to the onset of a charge density wave characteristic of half-filled conduction bands.[25]

Kharton et al.[26] studied $La_2Ni_{1-x}Fe_xO_{4\pm\delta}$ (x = 0.02 and 0.10) and $La_2Ni_{0.88}Fe_{0.02}Cu_{0.10}O_{4+\delta}$. Their studies showed that the electrical conductivity for these compositions increased with the substitution of iron, but the electrical conductivity slightly decreased with copper substitution. $La_{2-x}A_xNiO_4$ (A = Ca, Sr, and Ba) system has been investigated by Tang et al.,[27] and they have reported that the solubility limit was $0 \leq x \leq 0.6$ for Ca, $0 \leq x \leq 1.5$ for Sr, and $0 \leq x \leq 1.1$ for Ba. They have also found that both $La_{2-x}Ca_xNiO_4$ and $La_{2-x}Ba_xNiO_4$ compositions exhibited semiconducting behavior for all values of x. Moreover the $La_{2-x}Sr_xNiO_4$ compositions for $x < 0.6$ were reported to be semiconductor from room temperature up to 800 K. However, the compositions with $x > 0.6$ showed a transition temperature from semiconductor to metal, in which the transition temperature decreased as x increased. For $x > 1.3$, no such transition was identified from room temperature to 800 K. For $n = 2$ RP, the substitution of lanthanum by calcium on $La_{3-x}Ca_xNi_2O_{7-\delta}$ was reported by Nedilko et al.[28] A single phase has been obtained in the compositions for $0 \leq x \leq 0.8$. In addition, Ca dopant reduced the mean oxidation state of nickel ion from 2.63 ($x = 0$) to 2.15 ($x = 0.8$). Mogni et al.[29] reported that the electrical conductivity of the $La_{0.3}Sr_{2.7}FeNiO_{7-\delta}$ sample is higher than that of the $La_{0.3}Sr_{2.7}Fe_2O_{7-\delta}$ phase. The electrical conductivity of cobalt doped on Ni site of $La_4Ni_{3-x}Co_xO_{10\pm\delta}$ ($0.0 \leq x \leq 3.0$) was measured by Amow et al.[30] They have shown that the overall conductivity decreased, as x increased to $x = 2.0$. Conversely, the conductivity is found to increase with the higher amount of Co, that is, $x > 2.0$. Nagell et al.[31] have investigated the structural and magnetic properties of $La_4(Co_{1-x}Ni_x)_3O_{10+\delta}$ ($0 \leq x \leq 1$). They found the structure to be monoclinic with $P2_1/a$ symmetry. $La_4Co_3O_{10}$ was found to be as an anti-ferromagnetic semiconductor, where $La_4Ni_3O_{10}$ as a paramagnetic metal. Several experimental as well as theoretical studies have been made so far on the electrical and magnetic properties of $La_4Ni_3O_8$. However, the effect of dopant on the La site of the system has hitherto not been reported. As one can expect exotic behavior such as valence-state transition, magnetic transitions, insulator-to-metal transitions, etc, by electron/hole doping, we investigated the role of hole doping on crystal structure, electronic structure, and magnetic properties of $La_4Ni_3O_8$ using state-of-the-art density functional theoretical calculations.

■ STRUCTURAL ASPECTS

$La_4Ni_3O_8$ crystallizes in a body-centered tetragonal structure[3] with space group *I*4/*mmm* (No. 139). As appeared in Figure 1, this structure comprises of triple NiO_2 infinite layers separated by La^{3+} cations without oxygen, bringing planar nature to the crystal structure. These triple NiO_2 layers are separated from each other by $La/O_2/La$ fluorite-type layers. The NiO_2 trilayer is made of two types of Ni. The type-1 nickel (Ni1) and type-2 nickel (Ni2) are in inner and outer NiO_2 planes, respectively. Using the experimentally determined structural parameters as input, structural optimization was performed for $La_4Ni_3O_8$ as well as for Sr-substituted $La_4Ni_3O_8$. The experimental lattice parameters are well-reproduced by our GGA+*U* calculations with only −0.5% variation in equilibrium volume and 0.17% variation in the Ni−Ni and Ni−O bond lengths in $La_4Ni_3O_8$. No siginificant structural changes were observed when U_{eff} is changed from 0 to 5 eV. The theoretically optimized structural parameters are compared with available experimental values in Table 1. The inner NiO_2 plane has an intralayer Ni1−O separation of 1.9817 Å and an O−Ni1−O angle of 180°, whereas the external NiO_2 plane has a little distortion with an intralayer Ni2−O separation of 1.9819 Å bringing the O−Ni2−O angle to ~178°. The presently calculated interlayer Ni1−Ni2 distance at the equilibrium volume is 3.2578 Å, which is

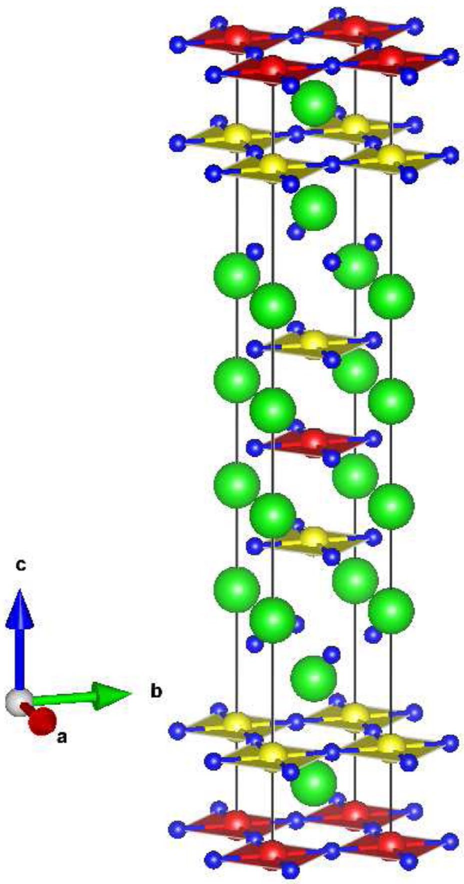

Figure 1. The crystal structure of $La_4Ni_3O_8$. The NiO_4 square planes are in red and yellow with Ni1 and Ni2 atoms in the centers, respectively. La atoms are represented as green spheres (big), and O atoms are blue spheres (small).

Table 1. Structural Parameters for the Tetragonal $La_{4-x}Sr_xNi_3O_8$

	$x^a = 0$	$x = 1$	$x = 2$	$x = 3$
V^b	409.56 411.12^c	403.38	407.50	411.62
a^b	3.9642 3.9708^c 3.9705^d	3.9441	3.9575	3.9708
c^b	26.0621 26.1057^c 26.103^d	25.9305	26.0184	26.1057

[a] x stands for Sr substitution, which varies from 0 to 3; [b] whereas a and c represent the lattice parameters of the tetragonal structure (in Å), and V represents the volume of the unit cell (in $Å^3$). [c] Reference 3. [d] Reference 38.

consistent with the previously reported value by Ting Liu et al.,[14] obtained using similar structural optimization approach. The structural parameters for undoped and Sr doped $La_4Ni_3O_8$ are given in Table 1.

■ COMPUTATIONAL DETAILS

The calculations presented in this paper were performed using the standard full-potential linearized augmented plane-wave method implemented in the WIEN2k[32,33] code based on density functional theory.[34] The room-temperature powder neutron diffraction lattice parameters and the atomic positions were taken from ref 3. For all calculations, the muffin-tin radii (R_{mt}) were chosen as 2.32, 2.35, 1.97, and 1.75 au for Sr, La, Ni, and O, respectively. The cutoff parameter $R_{mt}K_{max}$ was set to 7.0. To ensure the convergence for the Brillouin zone integration, 1000 k-points were used over the irreducible wedge of the first Brillouin zone (IBZ). Self-consistency was accomplished by demanding the convergence of the total energy to be smaller than 1×10^{-5} Ry/cell. This is comparable to a charge convergence to below 1×10^{-4} electrons/atom. The generalized gradient approximation (GGA) using the parametrized scheme of Perdew et al.[35] was utilized for the exchange-correlation potential. The low-dimesional transition-metal oxides such as $La_4Ni_3O_8$ will have strong Coulomb correlation effect arising from the transition-metal 3d states. To properly describe the strong electron correlation associated with Ni 3d states, the GGA+U method was used in the "fully localized limit" (FLL).[36] Here $U_{eff} = U - J$ (U and J are on-site Coulomb repulsion and exchange interaction, respectively) was used instead of U. For nickelates, the reasonable range of the U parameter is 4−8 eV.[2,10,11,13] So, the results presented below were calculated with U_{eff} = 5 and 6 eV. To clarify the magnetic ground state, 2 × 2 × 1 supercell calculations were performed for one FM (shown in Figure 2a) and three AFM spin configurations. For AFM configuration, at least three different magnetic arrangements are possible according to interplane and intraplane coupling, specifically: (i) With interplane AFM coupling and intraplane FM coupling, the *A*-AFM structure emerges as shown in Figure 2b. (ii) The inverse structure of *A*-AFM, where the interplane coupling is FM and the intraplane coupling is AFM, is known as *C*-AFM (Figure 2c). (iii) If both the interplane and intraplane couplings are AFM, the *G*-AFM[37] structure emerges as shown in Figure 2d.

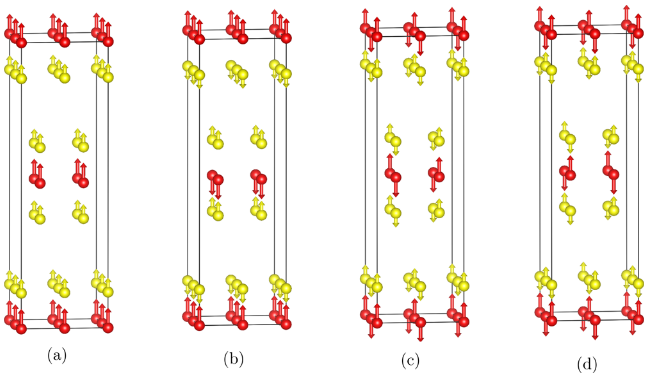

Figure 2. Schematic representation of (a) FM, (b) *A*-AFM, (c) *C*-AFM, and (d) *G*-AFM ordering in a 2 × 2 × 1 supercell of tetragonal $La_4Ni_3O_8$; only Ni ions are shown. Note that the supercell consists of two types of Ni atoms denoted as Ni1 (red spheres) and Ni2 (yellow spheres), where Ni1 (having large arrows) has larger magnetic moment than Ni2 (having small arrows).

■ RESULTS AND DISCUSSIONS

Electronic and Magnetic Structure of Undoped $La_4Ni_3O_8$. The relative total energies of various spin configurations with respect to the ground-state configuration are calculated and summarized in Table 2. Our GGA calculations for all the considered spin configurations show metallic features, which is in disagreement with the experimental observation.[11] However, within GGA, the FM and *A*-AFM states are found to have lower energies than *C*-AFM state by 35 and 41 meV, respectively, as given in Table 2. The *G*-AFM state has a very high energy relative to all the considered magnetic configurations and is ~250 meV higher than the ground state, *A*-AFM. It is well-known that $La_4Ni_3O_8$ is a strongly correlated material. Owing to the limitation of usual density-functional calculations in predicting the properties

Table 2. Calculated Total Energies ΔE (meV/f.u.) Relative to the Lowest Energy States, the Magnetic Moments M_s (μ_B) at the Ni Sites, Band Gap E_g (eV) Values for Different Magnetic States Depend on the $U_{\rm eff}$ (eV) Values for $La_4Ni_3O_8$

$U_{\rm eff}$		FM	*A*-AFM	*C*-AFM	*G*-AFM
0	ΔE	5.9	0	40.95	253.83
	M_s	0.52/0.54	0.50/0.52	0.27/0.29	0.21/0.28
		0.52/0.54^a	0.57/0.52^a	0.29/0.27^a	
	E_g	metal	metal	metal	metal
5	ΔE	189.28	179.46	0	
	M_s	0.77/0.75	0.81/0.78	1.44/1.29	
		0.79/0.77^a	0.83/0.81^a	1.44/1.29^a	
		0.79/0.77^b	0.8/0.8^b	1.44/1.29^b	
	E_g	metal	metal	0.7	
				0.7^b	
6	ΔE	340.65	330.73	0	
	M_s	0.80/0.79	0.83/0.80	1.50/1.34	
		0.82/0.79^a	0.85/0.80^a	1.49/1.35^a	
				1.39/1.25^c	
	E_g	metal	metal	0.58	

[a] Reference 14. [b] Reference 7. [c] Reference 39.

of strongly correlated materials, insulating transition-metal oxides are generally predicted to be metals. This can be remedied by going beyond GGA such as GGA+U calculations. Hence, to account for the strong correlation effect in $La_4Ni_3O_8$, we included a Hubbard U into the Hamiltonian matrix and optimized the crystal structure for different magnetic structures using $U_{\rm eff}$ values of 5 eV as well as 6 eV. Within GGA+U, the calculation for *G*-AFM state does not converge, consistent with observation made by Ting Liu et al.[14] The calculated total energy and magnetic moments are listed in Table 1 except for the unconverged *G*-AFM state. The results remain qualitatively unchanged for $U_{\rm eff}$ values of 5 and 6 eV. Within GGA+U ($U_{\rm eff}$ = 5 eV), the *C*-AFM is the most stable configuration. The energy of *C*-AFM is ∼190 and 180 meV lower than the FM and *A*-AFM states, respectively. Also only the *C*-AFM configuration shows insulating behavior, which is consistent with the experimental findings. As covalent bonding is present between O 2p and Ni 3d orbitals, one could expect induced magnetic moment in the oxygen site. Our GGA+U calculation shows that, in the FM configuration for the undoped system, the magnetic moment present in the neighboring oxygen sites is 0.040, 0.039, and 0.002 μ_B, respectively, for O1, O2, and O3 atoms. As O1 and O2 are the oxygens present within the square-planar layer, they have a strong hybridization with Ni1 and Ni2, respectively. But O3 atom is present in the fluorite-type layer, which has no direct interaction with Ni atoms resulting in lower magnetic moment than the other two oxygens. The magnetic moments at the oxygen ions are found to be directed parallel to the minority-spin channel of Ni atoms.

One can usually expect large magnetic moment in the FM configuration, compared to the AFM configuration. In the present system we found that the magnetic moment in the Ni site for the FM configuration is comparable with that of *A*-AFM configuration. So the magnetic moment in the Ni site is influenced by the intralayer FM coupling between the Ni atoms. It is expected that, because of the layered structure of this system, the interlayer FM coupling will be weaker, and hence it may not influence the ground-state magnetic configuration. Our calculation shows that the interlayer FM coupling is very important to understand the stability of this system. In fact, the calculated magnetic moments in the Ni sites are very small in the case of *C*-AFM if the strong correlation effect is not included into the calculation through the U parameter. However, when we include strong Coulomb correlation into the calculation using GGA+U method, the magnetic moment at the Ni sites increases by several orders of magnitude in the *C*-AFM case. But the magnetic moment enhancement in the FM and *A*-AFM configuration is not that large as compared to the enhancement in *C*-AFM configuration. Most importantly, the experimentally found insulating behavior could be reproduced only when we include the strong correlation effect into the calculation. This clearly indicates that the origin of the insulating behavior in $La_4Ni_3O_8$ is not only due to the FM coupling between the layers but also due to the Coulomb correlation effect present in the system.

To understand the role of various magnetic orderings on electrical properties of $La_4Ni_3O_8$ we analyzed in detail the total and orbital-projected density of states (DOS) for this system in different magnetic configurations. The optimized structure for $La_4Ni_3O_8$ shows that both Ni1 and Ni2 are surrounded by four oxygen atoms in square-planar coordination. In an ideal square-planar crystal field, Ni 3d splits into the highest level x^2-y^2, middle levels consist of doubly degenerate z^2, and xy and the lowest levels consist of doubly degenerate yz, xz.[40] But, because of the layered structure of $La_4Ni_3O_8$, the energy of z^2 orbital is lowered. This is because of the reduced Coulomb repulsion for both Ni1 and Ni2 in the layers.[41] In such a picture, $d_{x^2-y^2}$ orbital of the Ni atom will form σ bond with O-2p orbitals. Because of the absence of apical oxygens d_{z^2} orbital forms weak π bond with O-2p orbitals. As the xy, yz, and xz orbitals are fully occupied, they hybridize weakly with O-2p orbitals of oxygen atom (Figure 4). The orbital-projected DOS analysis shows that the hybridization between Ni-3d and O-2p orbitals is important to explain the electronic structure of $La_4Ni_3O_8$. Our site- and angular-momentum-projected DOS for the ground-state *C*-AFM configuration shows that the DOS for Ni-3d and O-2p orbitals are degenerate in the energy range from −6 eV to E_F, which ensures covalent bonding between these two atoms. Because of this strong covalent hybridization of Ni 3d with neighboring O 2p states, the calculated DOS curves shown in Figure 5 show broad features. To understand the effect of square-planar geometry on Ni 3d orbitals, the orbital-projected DOS is plotted, which is shown in Figure 4.

Let us first analyze the results from the calculations corresponding to the FM configuration. The orbital-projected DOS obtained from the GGA+U ($U_{\rm eff}$ = 5 eV) is shown in Figure 4 for the FM configuration. $La_4Ni_3O_8$ exhibits half metallicity in the FM state as seen in the Figure 3 and Figure 4 (with metallic character in up-spin channel and semiconducting character with a band gap of 0.86 eV in the down-spin channel). The majority-spin x^2-y^2 states with broad band features and significant bands from O 2p states cross the Fermi level (not shown) resulting in half-metallicity. As seen from the Figure 4, the 3d DOS distribution for the Ni1 and Ni2 have almost the same shape and also have the same electron occupation. This implies that Ni atoms have a charge-homogeneous solution with the average valence of $Ni^{+1.33}$ in this system. Consistent with this viewpoint, the calculated magnetic moment in both the Ni sites are almost the same. It can be noted that the presence of half metallic behavior in the FM configuration disagrees with the experimental observation of insulating behavior. From the Figure 4, we found that the

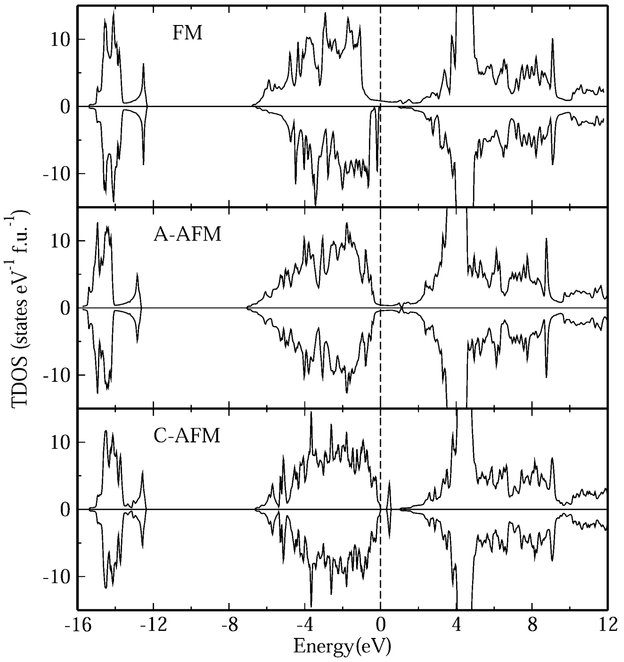

Figure 3. Total DOS for $La_4Ni_3O_8$ in FM, *A*-AFM, and *C*-AFM states obtained from GGA+*U* calculations with U_{eff} = 5 eV.

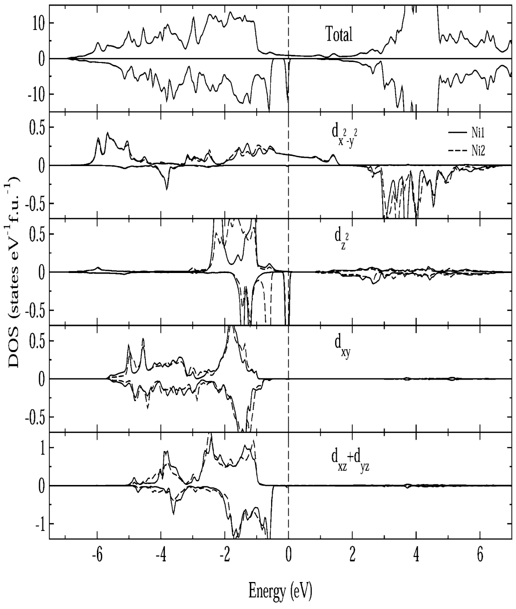

Figure 4. Orbital projected DOS of $La_4Ni_3O_8$ in FM configuration calculated using GGA+*U* method with U_{eff} = 5 eV.

majority-spin x^2-y^2 orbitals of Ni1 and Ni2 are partially (2/3) occupied, while the minority-spin x^2-y^2 orbitals of both the ions are nearly empty. The other 3d orbitals are completely filled, which suggests that both the ions hold the low-spin state in the FM configuration. Each two-thirds occupied up-spin x^2-y^2 band of Ni1 and Ni2 ions contribute 2/3 μ_B to the total calculated moment of 2 μ_B per formula unit. As the $d_{x^2-y^2}$ orbital has an in-plane orientation, an *A*-type AFM state (intralayer FM and interlayer AFM within the trilayer) turns out to have a similar DOS characteristic (not shown here) as that of FM configuration mentioned above. So the *A*-AFM configuration also possesses a low-spin metallic solution. From the calculated total energy for $La_4Ni_3O_8$ in various magnetic configurations given in Table 2 it is clear that the *C*-AFM state is the most stable state within GGA+*U*. As the Fermi level falls in the gap for both spin channels, the *C*-AFM configuration exhibits an insulating feature (0.7 eV with U_{eff} = 5 eV). The valence band DOS of $La_4Ni_3O_8$ is primarily derived from Ni 3d and O 2p admixture. The negligibly small DOS contribution in the valence band (VB) at the La site indicates pronounced ionic bonding between La and other constituents. The almost same topology of the DOS profile for the two Ni sites strongly suggests average valence states for both Ni atoms. In Figure 5 we displayed the angular momentum projected DOS for La, Ni, and O atoms in $La_4Ni_3O_8$. The s and p states of Ni and d states of O have negligible contribution (visible only after significant magnification) in the VB in the vicinity of E_F.

The d states of Ni atoms and p states of O1 and O2 atoms distributed from −6 eV to E_F. This implies that the Ni d and O

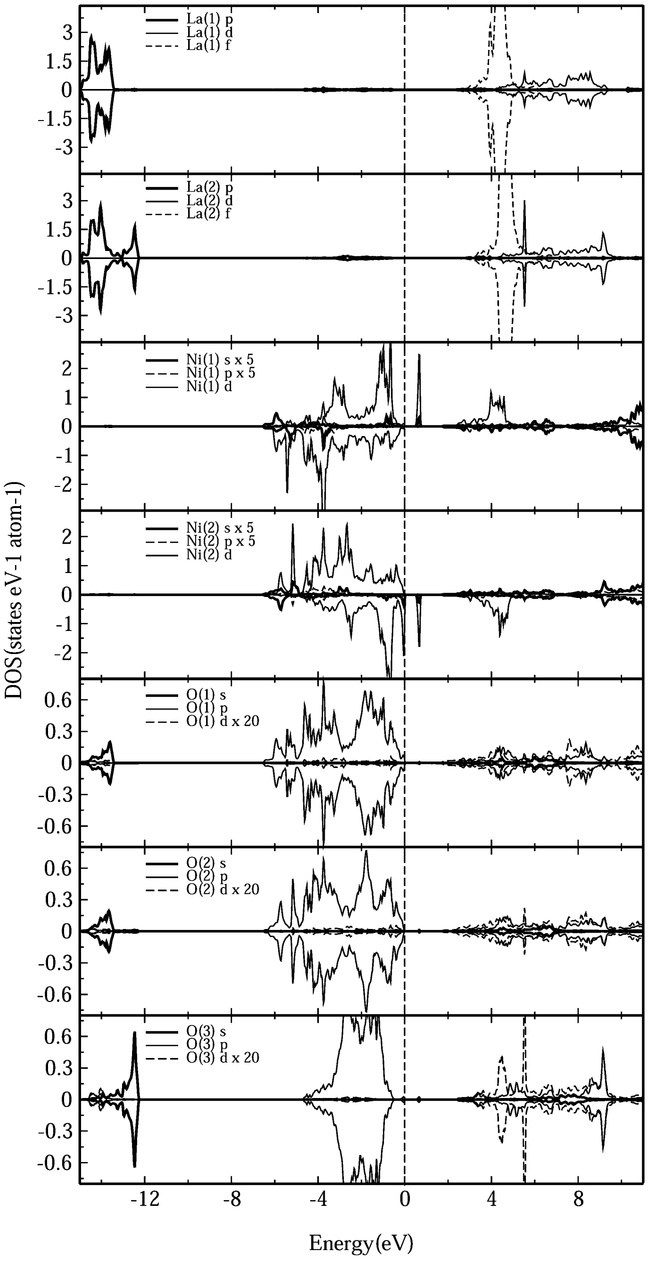

Figure 5. Site and angular-momentum projected DOS for $La_4Ni_3O_8$ *C*-AFM configuration calculated using GGA+*U* method with U_{eff} = 5 eV.

p states are strongly hybridized. The O 2s states for O1 and O2 are well-localized and are present around −15 eV. As O3 is present in the La2/(O3)$_2$/La2 fluorite-type layers, it has somewhat different DOS characteristics as compared to the square-planar oxygens (O1 and O2). The 2s states for O3 atom are present in a higher state as compared to that for the other two oxygen atoms. The *xy*, *yz*, and *xz* orbitals of Ni atoms are fully occupied and localized in a narrow energy range, indicating that they hybridize weakly with the O 2p orbitals. Because of the absence of apical oxygens, the d_{z^2} orbital forms pdπ bonding with O 2p orbital. The $d_{x^2-y^2}$ orbital hybridizes strongly with the O 2p orbital within the layers to produce broad bands. The Ni 3d states produce narrow bands, which indicate the strong correlation effect in La$_4$Ni$_3$O$_8$. As shown in Figure 6, the majority-spin DOS for d_{z^2} orbital is completely occupied, whereas the DOS for the corresponding orbital in the minority spin state is partially occupied. It may be noted that the occupied and unoccupied levels are separated by a gap of ∼0.7 eV. However, it is interesting to note that our GGA+*U* calculations give rise to some intermediate band-gap states. The present result is, to the best of our knowledge, the first to point out the occurrence of intermediate energy states in the band gap of La$_4$Ni$_3$O$_8$. Intermediate band gap oxides attract much attention due to their potential applications in solar cells.[42,43] The orbital-projected DOS shows that these intermediate states are originating from d_{z^2} electrons from both the Ni ions, which may be induced by the correlation effect.

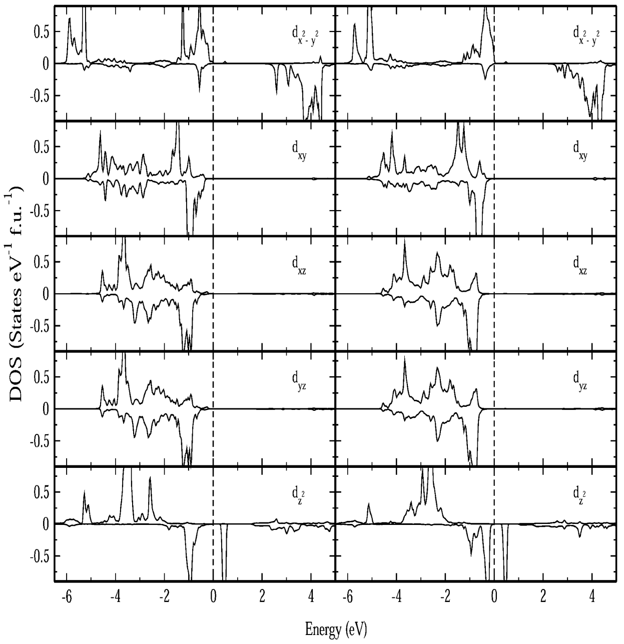

Figure 6. Orbital-projected DOS for Ni (Ni1 left and Ni2 right) in *C*-AFM state for La$_4$Ni$_3$O$_8$ calculated by GGA+*U* method with $U_{\mathrm{eff}} = 5$ eV.

Let us now turn our attention to the valence and spin states of Ni ions in La$_4$Ni$_3$O$_8$ in the ground-state magnetic configuration. Because of the Coulomb repulsion induced by four d_{z^2} electrons of two Ni2 ions within the trilayer along the c-axis, one Ni1 d_{z^2} electron will be excited to the corresponding $d_{x^2-y^2}$ orbital. As a result all the nickel ions would have half-filled $d_{x^2-y^2}$ orbital, and ultimately *C*-AFM would be in an HS state. Because of the intralayer coupling present in *C*-AFM configuration, the $d_{x^2-y^2}$ bandwidth decreases significantly. (See FM and *C*-AFM orbital-projected DOS given in Figure 4 and Figure 6, respectively, in the manuscript for comparison.) This would force La$_4$Ni$_3$O$_8$ to be a Mott insulator with a strong intralayer AFM coupling. Note that the AFM Mott insulating ground state agrees with experiments.[11,18] The Hubbard *U* parameter stabilizes the HS AFM state and opens the Mott insulating gap. Now both the $d_{x^2-y^2}$ and d_{z^2} orbitals should have one hole in the minority spin state, which can be seen from the orbital-projected DOS given in Figure 6. From the integrated orbital-projected DOS, we calculated the occupation numbers for the majority spin of $d_{x^2-y^2}$ and d_{z^2} orbitals of Ni1 ion, which are 0.95e and 0.92e, respectively, as expected. But the strong hybridization between Ni 3d and O 2p orbitals induces 0.17e and 0.36e for the minority spins states of the $d_{x^2-y^2}$ and d_{z^2} orbitals, respectively. All other d-orbitals of Ni1 ions are found to be fully occupied. Similarly, for the two Ni2 ions present in the trilayer, the $d_{x^2-y^2}$ majority (minority) spin state and the d_{z^2} majority (minority) spin state have the occupations numbers of 0.92e (0.16e) and 0.89e (0.45e), respectively. As a consequence of this, the minority-spin d_{z^2} electron of Ni2 can readily hop to the formally empty minority-spin d_{z^2} orbital of Ni1 ion. This stabilizes the interlayer FM coupling within the trilayer. The band originating from x^2-y^2 states in the *C*-AFM configuration is narrower compared to that in the FM configuration. This reduction in bandwidth is due to the weaker intralayer AFM coupling. In *C*-AFM configuration, the Ni atoms align antiferromagnetically due to linear Ni−O−Ni superexchange interactions.[44] The $d_{x^2-y^2}$ orbital of Ni atoms interact through the same oxygen p_x/p_y orbital causing antiparallel spins on neighboring Ni atoms, and this could explain the stabilization of the AFM configuration over the FM configuration.

The next puzzle is the understanding the origin of comparatively larger moment at the Ni1 site than that in the Ni2 site. If an oxygen atom is removed from a Ni−O−Ni configuration with bond angle 180°, the Ni atoms repel each other due to the electrostatic force, and the neighboring O atoms collectively move toward the vacancy to screen the repulsion. The optimized crystal structure parameters show that the Ni atoms of the Ni1 site are surrounded by four base-plane O atoms at a distance of 1.9817 Å and that the corresponding distance is 1.9819 Å in case of Ni2 site. These findings strongly suggest that the bonding interaction between Ni and O is stronger in the Ni1O$_4$ coordination than that in Ni2O$_4$ coordination. Hence, compared with the local surrounding of Ni2O$_4$, relatively more of the electrons in the Ni1O$_4$ subunits are participating in bonding rather than in magnetism. Since the bond lengths are almost similar for Ni1−O and Ni2−O, the magnetic moments at Ni1 and Ni2 are expected to be the same. But our calculation shows that the magnetic moment at the Ni1 site is 1.44 μ_B, which is comparatively larger than that at the Ni2 site (1.29 μ_B). This is because of the small distortion in the Ni2O$_4$ site for which the Ni−O−Ni bond angle is 178° versus 180° in the case of Ni1O$_4$. Because of the reduction in bond angle, the Ni2−O−Ni2 superexchange is hindered resulting in a lower magnetic moment at the Ni2 site.

Role of Hole-Doping La$_4$Ni$_3$O$_8$. To understand the changes in the electronic structure and magnetic properties of La$_4$Ni$_3$O$_8$ due to hole doping, we considered divalent Sr substitution (hole doping) at the La site. We performed calculations for this hole-doped system in different magnetic configurations similar to the undoped case mentioned above, adopting the similar approach. As there are several possibilities to replace La with Sr in $La_4Ni_3O_8$ we substituted La by Sr atom through supercell approach such that the Sr will locate with respect to the plane in the middle of the square spanned by the four Ni ions in the supercell.

Structural Changes. No systematic composition dependence of the parameters was observed, which can be seen from Table 1. But the increase in the lattice parameters from $x = 1$ to $x = 3$ can be understood as follows. The ionic radius of Sr^{2+} is slightly larger than that of La^{3+}. Hence, when La^{3+} is replaced by Sr^{2+} a negative chemical pressure acts primarily on the NiO_2 planar sub units, which increases the Ni−O−Ni bond angles. To compensate for the local repulsion between overlapping charge densities, the Ni−O bond lengths increase. In the case of $La_{4-x}Sr_xNi_3O_8$, for $x = 1$ and 2, Sr^{2+} occupies the vacancy created by the removal of La^{3+}. And in the case of $x = 3$, when the La/O_2/La layer is replaced by Sr, a further increase in the cell volume is noticed (Table 1). The observed c/a ratio has a maximum value at $x = 2$, because holes are first doped into the $d_{x^2-y^2}$ orbital for lower concentration and, then, additional holes are doped into the d_{z^2} orbital for higher concentration of Sr similar to the bilayer system investigated by Gopalkrishnan et al.[45] and Takeda et al.[46] Moreover, since Sr doping is equivalent to hole doping, the number of electrons contained in VB decreases with increasing Sr concentration. This leads to a systematic shift of E_F toward the lower-energy region of the DOS. As the size of Sr atom is not very different from La (ionic radii of Sr and La are 0.061 and 0.059 Å, respectively), the hole doping does not modify the structure of the parent material significantly, which can be seen from the optimized structural parameters given in Table 1. Because of the smaller electronegativity difference between Sr and La, the substitution of La with Sr will not have noticeable changes in the band structure except band filling originating from the hole-doping effect.

Changes in Electronic and Magnetic Structure by Hole Doping. As Sr is divalent and La is trivalent, removal of electrons from the NiO_4 sublattice is necessary to balance the charge deficiency introduced by the Sr substitution. Thus, VB shows an upward shift toward the Fermi energy as shown in Figure 8. From this figure it is clear that the small concentration of La substituted by Sr in $La_4Ni_3O_8$ significantly changes the electronic structure of the system. Our calculated DOS curves also show significant changes in the electronic structure of both types of Ni atoms due to the substitution of La by Sr as evident in Figure 7 and Figure 9. This indicates that hybridization and charge transfer effects play important roles in describing the electronic structure of $La_{4-x}Sr_xNi_3O_8$. As the stability of $La_{4-x}Sr_xNi_3O_8$ mainly originates from the covalent interaction between the Ni 3d and O 2p electrons, changing the d band filling of the Ni d states in the VB around the Fermi level at higher Sr concentration is expected to give rise to structural destabilization. This could explain why high Sr concentrations in $La_{2-x}Sr_xNiO_4$ could always bring oxygen vacancy as reported experimentally.[23] Hence it is expected that the higher Sr concentration in $La_4Ni_3O_8$ also stabilizes this system with oxygen vacancy.

The calculated partial DOS for $La_2Sr_2Ni_3O_8$ (with 50% Sr substitution) for the ground-state C-AFM configuration is given in Figure 8. From the DOS analysis we found that, except the localized states at ca. −12 to −14 eV derived from Sr, the DOS in the whole energy range is almost the same as that of $La_4Ni_3O_8$ irrespective of the Sr concentration. However, all the electronic states in the VB get shifted toward the higher energy upon Sr substitution as evident from the calculated DOS. This can be explained as follows. Since Sr doping is equivalent to removing one electron from the system, the number of electrons contained in the VB decreases with increasing amount of Sr concentration. This leads to a systematic shift of E_F toward the lower-energy region of DOS, if the system follows simple band filling effect. It may be noted that, similar to La, Sr also donates all its valence electrons to the host lattice and forms ionic bonding. Replacing La with Sr introduces hole states above the Fermi level and reduces the electron-per-atom ratio in $La_4Ni_3O_8$. If we assume that the rigid-band-filling principle works in this case, the reduction in the electron-per-atom ratio is equivalent to shifting E_F toward the lower-energy side of DOS. As there are not very many changes in the DOS topology with Sr substitution, one can conclude that Sr substitution will only change the valence electron count without influencing the hybridization interaction between Ni and O significantly. So we focus on the position of the Fermi level, width of the VB as well as conduction band, and bandgap changes as a function of Sr substitution, because they play a key role in the electrical, magnetic, and optical properties of the system.

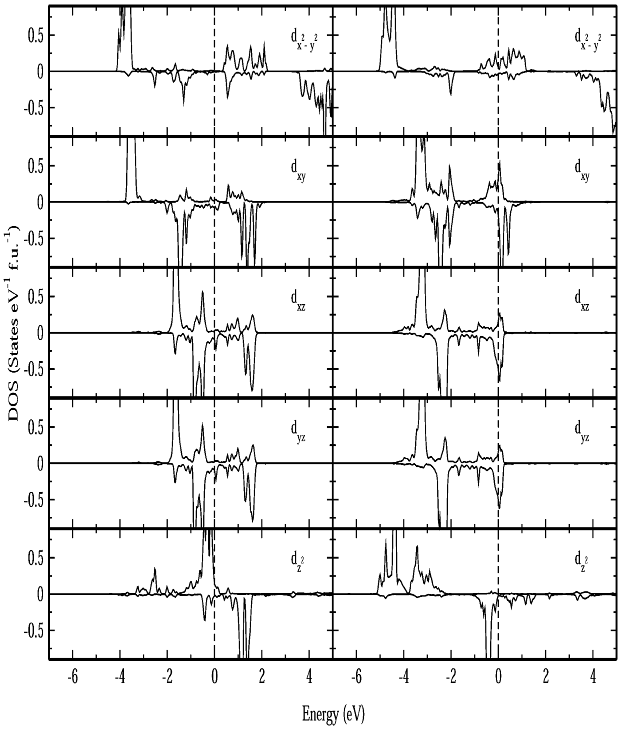

Figure 7. Orbital-projected DOS for Ni (Ni1 left and Ni2 right) close to Sr in C-AFM state for $La_3SrNi_3O_8$ calculated by GGA+U method with U_{eff} = 5 eV.

To understand the role of Sr substitution on electrical and magnetic properties of $La_4Ni_3O_8$ we plotted the orbital-projected DOS for the constituents with 25% Sr substitution (see Figure 7). The orbital-projected DOS shows that more of the d-DOS of the Ni1 site has moved toward the unoccupied site than that in Ni2 site. This is not surprising, because two Sr atoms are present as neighbors for Ni1, whereas the Ni2 is surrounded by only one Sr ion alone in $La_3SrNi_3O_8$. In this system, it is natural that Sr substitution adds one hole in the Ni sites resulting in increase of total oxidation states of both Ni ions from 4+ to 5+ state. As the radius of Sr^{2+} is (slightly) larger than that of La^{3+}, it is suggested that the Sr doping favors the

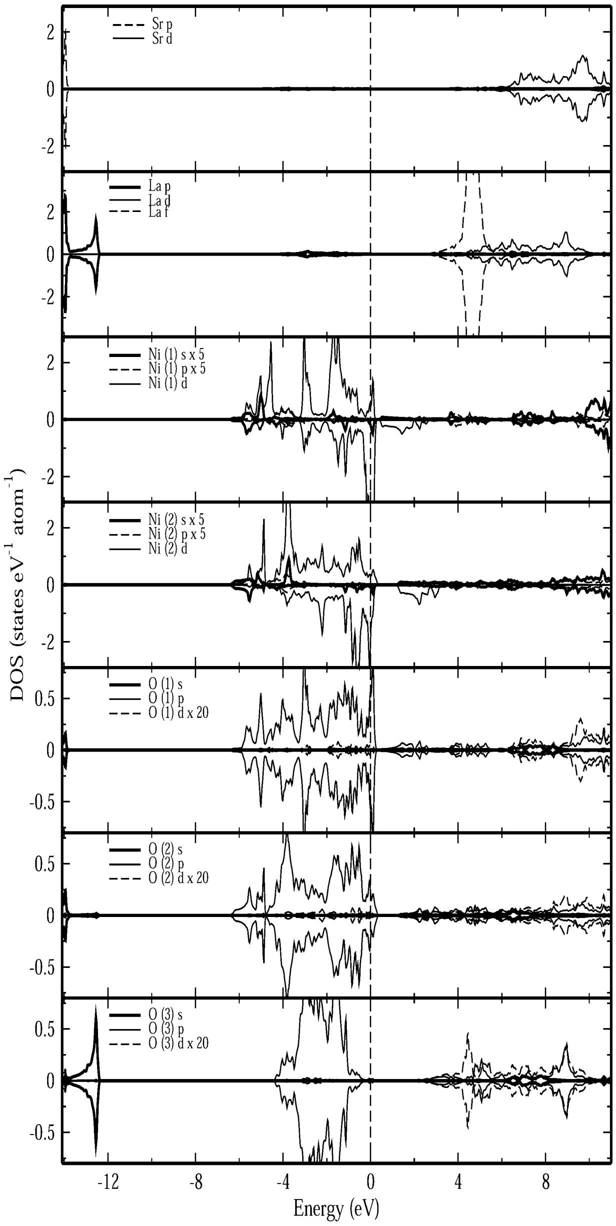

Figure 8. Partial DOS for *C*-AFM state of $La_2Sr_2Ni_3O_8$ calculated by GGA+*U* method with U_{eff} = 5 eV.

HS state in nickelates by the introduction of partial oxidation due to covalency effect.[37,47] As the doped system also possesses average valency (all Ni atoms are having almost equal moments), the partial oxidation state introduced by hole doping increases the average valency from +1.33 to +1.67; that is, Ni atoms will have HS with maximum magnetic moment of 1.67 μ_B. But these considerations correspond to the purely ionic model, the hybridization of Ni 3d orbitals with O 2p orbitals, and the resulting broad-band formation can significantly renormalize this ionic value. Hence the calculated magnetic moments are always smaller than the ideal ionic values mentioned above. It may be noted that we have not considered O nonstoichiometry in the present calculations. But in experiment one may expect oxygen deficiency in hole-doped systems or at high temperatures. Especially one can expect a disagreement between experiment and theory for $x > 0.5$, where the oxygen deficiency is known to increase significantly. From Figure 8, we can see that the reduction of electron population caused by hole-doping affects the electron distribution not only in Ni1 and Ni2 but also in O1 and O2 atoms. Because of the hole-doping, the Ni and O DOS cross the Fermi level bringing insulator-to-metal transition without affecting the AFM ordering.

According to Goodenough,[48] a change between FM and AFM states may be expected when the magnetic moment for the FM and AFM states is almost the same ($\mu_F \approx \mu_{AFM}$); the stable magnetic phase being the one that has the highest magnetic moment. Our calculated results are consistent with this viewpoint in the sense that the magnetic moments are found to be larger for the stable magnetic configuration (*C*-AFM) in $La_{4-x}Sr_xNi_3O_8$ (see Table 2 for magnetic moment of different magnetic configurations for $x = 0$). When we go from $La_3SrNi_3O_8$ to $LaSr_3Ni_3O_8$, the magnetic moment increases. The increase in magnetic moment as a function of hole doping originates from two reasons: First, owing to band-filling effects the hole-doping moves the Fermi level to the lower-energy side and thus enhances DOS at the Fermi level as well as the exchange splitting. Second, owing to the larger size of Sr^{2+} than La^{3+}, lattice is expanded for increased Sr substitution leading to reduced hybridization and increased band localization. As a result, the bands become narrow, which in turn enhances the spin polarization. Furthermore, the increased exchange splitting of the Ni 3d bands also enhances magnetic moment.

To understand the change in the magnetic properties of the Ni ions present in the vicinity of Sr or La atoms, spin-polarized Ni 3d DOS for Ni1 and Ni2 atoms closer to Sr and La are presented in Figure 7 and Figure 9 for the $La_3SrNi_3O_8$ and $LaSr_3Ni_3O_8$ cases, respectively. From this illustration it is clear that the d states for both Ni atoms are itinerant and also that both are participating in the magnetism. It is interesting to note that Ni atoms closer to Sr are more spin-polarized than those

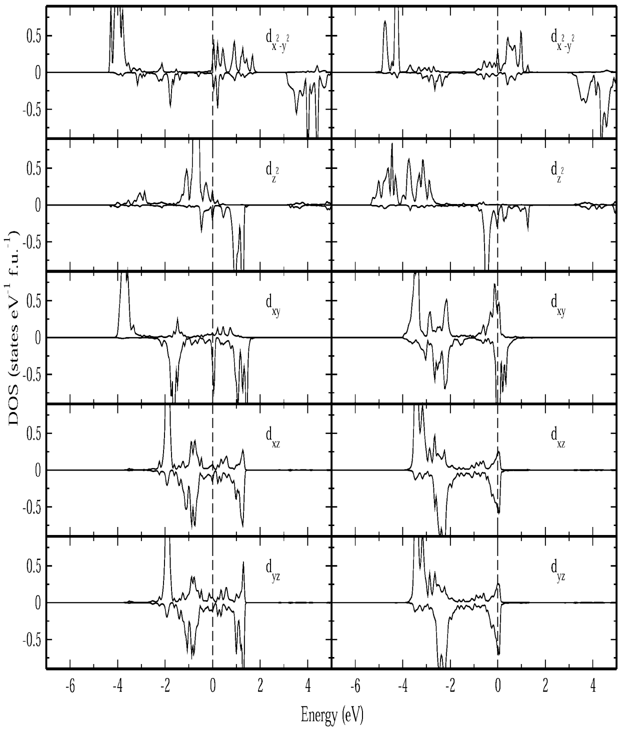

Figure 9. Orbital-projected DOS for Ni (Ni1 left and Ni2 right) close to Sr in *C*-AFM state for $LaSr_3Ni_3O_8$ calculated by GGA+*U* method with U_{eff} = 5 eV.

closer to La owing to the reasons discussed above. For the *C*-AFM ground state of $La_3SrNi_3O_8$, Ni1 closer to La possesses a magnetic moment of 1.50 μ_B, and that closer to Sr has 1.62 μ_B. Similarly, Ni2 closer to La possesses a magnetic moment of 1.34 μ_B, and those closer to Sr have 1.67 μ_B. In case of $x = 3$, that is, $LaSr_3Ni_3O_8$, the combined oxidation state of Ni atoms (Ni1 + 2Ni2) is increased from 4+ to 7+. So we can say that the Ni1 is in 3+ (d^7) and Ni2 is in 2+ (d^8) oxidation states. But magnetic moments obtained in none of the Ni site reflect these oxidation states (e.g., Ni^{2+} in HS is expected to be 1 μ_B). Therefore, signature for charge ordering with $d^7 + 2d^8$ ions is not observed in $LaSr_3Ni_3O_8$. The DOS distributions for both Ni sites are almost the same, and hence one can conclude that the Ni ions have an average valence of +2.33 ($d^{7.67}$), which leads to a maximum Ni moment of 2.33 μ_B. But in practice, oxides will not have a pure ionicity, and often they have mixed bonding behavior; that is, one can expect noticeable covalent hybridization between the transition metal and surrounding atoms. As a result, the spin moment reduces owing to the fact that some of the electrons participate in bonding rather than in magnetism. So, transition-metal sites mostly have noninteger value for the spin moments, and the surrounding atoms have small induced moments. Hence Ni1 closer to La is having a magnetic moment of 1.53 μ_B, and that closer to Sr has 1.58 μ_B for the 75% doped system. Similarly, Ni2 closer to La possesses a magnetic moment of 1.53 μ_B, and those closer to Sr have moment of 1.68 μ_B. This indicates that all the Ni atoms are in the HS state. Since $La_{4-x}Sr_xNi_3O_8$ in practice will have oxygen deficiency at higher Sr substitution, one may expect a lower magnetic moment than the calculated values depending on the oxygen stoichiometry. Our calculated magnetic moments are valid only for the system without any oxygen vacancy.

SUMMARY

We have made detailed investigation of the effect of hole doping on electronic structure and magnetic properties of trilayer $La_4Ni_3O_8$ using supercell approach. We have inferred the following:

1 Our calculations show that the *C*-AFM state is the ground state with the Ni ions in the HS state for $La_4Ni_3O_8$, in agreement with experimental observations.
2 We have identified strong covalent interactions between Ni and O within the NiO_2 square plane and ionic bonding between La and these building units in $La_4Ni_3O_8$.
3 According to our results, $La_4Ni_3O_8$ is a *C*-AFM insulator with strong interlayer coupling. This insulating state is caused by a strong Coulomb correlation effect and interlayer exchange coupling. Such strong interlayer coupling results from the HS occupation of Ni ions, where the d_{z^2} orbital gets occupied.
4 Our DOS calculation shows that in $La_4Ni_3O_8$ both the Ni ions are in an average valence state.
5 Our GGA+*U* calculations show intermediate band-gap states originating from d_{z^2} electrons from both the Ni ions, which may be induced by the correlation effect.
6 The hole doping brings insulator-to-metal transition without changing the *C*-AFM ordering.
7 No signature of charge ordering is seen after the hole doping, which indicates that the average valency is sustained though the oxidation state for both the Ni atoms increases with the dopant concentration.
8 The magnetic moment gets enhanced in all the Ni sites due to the increase in the oxidation state of the Ni ions for the hole-doping cases.

AUTHOR INFORMATION

Corresponding Author

*E-mail: raviphy@cutn.ac.in. Phone: +91-94890-54267.

Notes

The authors declare no competing financial interest.

ACKNOWLEDGMENTS

The authors are grateful to the Research Council of Norway for providing computing time at the Norwegian supercomputer facilities. This research was supported by the Indo-Norwegian Cooperative Program via Grant No. F. No. 58-12/2014(IC) and Research Council of Norway, Grant No. 221905 (FRIPRO). One of the authors (L.P.) gratefully acknowledges the Central Univ. of Tamil Nadu for the financial support.

REFERENCES

(1) Bednorz, J.; Müller, K. Possible high T_C superconductivity in the Ba−La−Cu−O system. *Z. Phys. B: Condens. Matter* **1986**, *64*, 189−193.

(2) Anisimov, V.; Bukhvalov, D.; Rice, T. Electronic structure of possible nickelate analogs to the cuprates. *Phys. Rev. B: Condens. Matter Mater. Phys.* **1999**, *59*, 7901−7906.

(3) Poltavets, V. V.; Lokshin, K. a.; Croft, M.; Mandal, T. K.; Egami, T.; Greenblatt, M. Crystal Structures of $Ln_4Ni_3O_8$ (Ln= La, Nd) Triple Layer T′-type Nickelates. *Inorg. Chem.* **2007**, *46*, 10887−10891.

(4) Poltavets, V. V.; Greenblatt, M.; Fecher, G. H.; Felser, C. Electronic Properties, Band Structure, and Fermi Surface Instabilities of Ni^{1+}/Ni^{2+} Nickelate $La_3Ni_2O_6$, Isoelectronic with Superconducting Cuprates. *Phys. Rev. Lett.* **2009**, *102*, 046405.

(5) Bednorz, J. G.; Müller, K. A. The Nobel Prize Lecture, 1987. Online at https://www.nobelprize.org/nobel_prizes/physics/laureates/1987/bednorz-muller-lecture.pdf.

(6) Torrance, J. B.; Lacorre, P.; Nazzal, a. I.; Ansaldo, E. J.; Niedermayer, C. Systematic study of insulator-metal transitions in perovskites $RNiO_3$ (R= Pr, Nd, Sm, Eu) due to closing of charge-transfer gap. *Phys. Rev. B: Condens. Matter Mater. Phys.* **1992**, *45*, 8209−8212.

(7) Liu, T.; Wu, H.; Jia, T.; Zhang, X.; Zeng, Z.; Lin, H. Q.; Li, X. G. Dimensionality-induced insulator-metal crossover in layered nickelates $La_{n+1}Ni_nO_{2n+2}$ (n= 2. 3, and ∞). *AIP Adv.* **2014**, *4*, 047132.

(8) Dagotto, E. Complexity in strongly correlated electronic systems. *Science* **2005**, *309*, 257−262.

(9) Blanca-Romero, A.; Pentcheva, R. Confinement-induced metal-to-insulator transition in strained $LaNiO_3/LaAlO_3$ superlattices. *Phys. Rev. B: Condens. Matter Mater. Phys.* **2011**, *84*, 195450.

(10) Pardo, V.; Pickett, W. E. Pressure-induced metal-insulator and spin-state transition in low-valence layered nickelates. *Phys. Rev. B: Condens. Matter Mater. Phys.* **2012**, *85*, 045111.

(11) Poltavets, V. V.; Lokshin, K. a.; Nevidomskyy, A. H.; Croft, M.; Tyson, T. a.; Hadermann, J.; Van Tendeloo, G.; Egami, T.; Kotliar, G.; Aproberts-Warren, N.; Dioguardi, A. P.; Curro, N. J.; Greenblatt, M. Bulk magnetic order in a two-dimensional $Ni^{1+}/Ni^{2+}(d^9/d^8)$ nickelate, isoelectronic with superconducting cuprates. *Phys. Rev. Lett.* **2010**, *104*, 206403.

(12) ApRoberts-Warren, N.; Dioguardi, A. P.; Poltavets, V. V.; Greenblatt, M.; Klavins, P.; Curro, N. J. Critical spin dynamics in the antiferromagnet $La_4Ni_3O_8$ from La139 nuclear magnetic resonance. *Phys. Rev. B: Condens. Matter Mater. Phys.* **2011**, *83*, 014402.

(13) Pardo, V.; Pickett, W. E. Quantum confinement induced molecular correlated insulating state in $La_4Ni_3O_8$. *Phys. Rev. Lett.* **2010**, *105*, 1−4.

DOI: 10.1021/acs.inorgchem.6b01938
Inorg. Chem. 2016, 55, 11898−11907

(14) Liu, T.; Zhang, G.; Zhang, X.; Jia, T.; Zeng, Z.; Lin, H. Q. Electronic structure and magnetism of $La_4Ni_3O_8$ from first principles. *J. Phys.: Condens. Matter* **2012**, *24*, 405502.

(15) Andersen, O. K.; Jepsen, O. Explicit, first-principles tight-binding theory. *Phys. Rev. Lett.* **1984**, *53*, 2571−2574.

(16) Andersen, O. K.; Saha-Dasgupta, T. Muffin-tin orbitals of arbitrary order. *Phys. Rev. B: Condens. Matter Mater. Phys.* **2000**, *62*, 219−222.

(17) Sarkar, S.; Dasgupta, I.; Greenblatt, M.; Saha-Dasgupta, T. Electronic and magnetic structures of bilayer $La_3Ni_2O_6$ and trilayer $La_4Ni_3O_8$ nickelates from first principles. *Phys. Rev. B: Condens. Matter Mater. Phys.* **2011**, *84*, 180411.

(18) Cheng, J.-G.; Zhou, J.-S.; Goodenough, J.; Zhou, H.; Matsubayashi, K.; Uwatoko, Y.; Kong, P.; Jin, C.; Yang, W.; Shen, G. Pressure Effect on the Structural Transition and Suppression of the High-Spin State in the Triple-Layer T′-type $La_4Ni_3O_8$. *Phys. Rev. Lett.* **2012**, *108*, 236403.

(19) Cava, R.; Batlogg, B.; Palstra, T.; Krajewski, J.; Peck, W., Jr; Ramirez, A.; Rupp, L., Jr Magnetic and electrical properties of $La_{2-x}Sr_xNiO_{4\pm\delta}$. *Phys. Rev. B: Condens. Matter Mater. Phys.* **1991**, *43*, 1229.

(20) Chokkha, S.; Kuharuangrong, S. Synthesis and Characterization of $La_{4-x}Sr_xNi_3O_{10\pm\delta}$ Ruddlesden-Popper Structure. *Key Eng. Mater.* **2014**, 264−273.

(21) Takagi, H.; Batlogg, B.; Kao, H.; Kwo, J.; Cava, R.; Krajewski, J.; Peck, W. Systematic evolution of temperature-dependent resistivity in $La_{2-x}Sr_xCuO_4$. *Phys. Rev. Lett.* **1992**, *69*, 2975−2978.

(22) Dicarlo, J.; Bularzik, J.; Navrotsky, A. A thermochemical study of $La_{2-x}A_xCuO_{4-y}$ (A = Ba, Sr, Ca, Pb). *J. Solid State Chem.* **1992**, *96*, 381−389.

(23) Sreedhar, K.; Honig, J. M. Low-Temperature Electron Transport Properties of $La_{2-x}Sr_xNiO_4$ with $0.5 < x < 1.3$. *J. Solid State Chem.* **1994**, *111*, 147−150.

(24) Arbuckle, B. W.; Ramanujachary, K.; Zhang, Z.; Greenblatt, M. Investigations on the structural, electrical, and magnetic properties of $Nd_{2-x}Sr_xNiO_{4+\delta}$. *J. Solid State Chem.* **1990**, *88*, 278−290.

(25) Takeda, Y.; Nishijima, M.; Imanishi, N.; Kanno, R.; Yamamoto, O.; Takano, M. Crystal chemistry and transport properties of $Nd_{2-x}A_xNiO_4$ (A = Ca, Sr, or Ba, $0 \leq x \leq 1.4$). *J. Solid State Chem.* **1992**, *96*, 72−83.

(26) Kharton, V.; Viskup, A.; Naumovich, E.; Marques, F. B. Oxygen ion transport in La_2NiO_4-based ceramics. *J. Mater. Chem.* **1999**, *9*, 2623−2629.

(27) Tang, J.; Dass, R.; Manthiram, A. Comparison of the crystal chemistry and electrical properties of $La_{2-x}A_xNiO_4$ (A = Ca, Sr, and Ba). *Mater. Res. Bull.* **2000**, *35*, 411−424.

(28) Nedilko, S.; Kulichenko, V.; Dziazko, A.; Zenkovich, E. Oxygen nonstoichiometry and properties of lanthanum nickelates $La_{3-x}Ca_xNi_2O_{7-\delta}$ ($0 \leq x \leq 2.0$). *J. Alloys Compd.* **2004**, *367*, 251−254.

(29) Mogni, L.; Prado, F.; Caneiro, A.; Manthiram, A. High temperature properties of the n= 2 Ruddlesden−Popper phases $(La,Sr)_3(Fe,Ni)_2O_{7-\delta}$. *Solid State Ionics* **2006**, *177*, 1807−1810.

(30) Amow, G.; Au, J.; Davidson, I. Synthesis and characterization of $La_4Ni_{3-x}Co_xO_{10\pm\delta}$ ($0.0 \leq x \leq 3.0$, $\Delta x = 0.2$) for solid oxide fuel cell cathodes. *Solid State Ionics* **2006**, *177*, 1837−1841.

(31) Nagell, M. U.; Kumar, S.; Sørby, M. H.; Fjellvåg, H.; Sjåstad, A. O. Structural and magnetic aspects of $La_4(Co_{1-x}Ni_x)_3O_{10+\delta}$ ($0 \leq x \leq 1$). *Phase Transitions* **2015**, *88*, 979−990.

(32) Blaha, P.; Schwarz, K.; Madsen, G.; Kvasnicka, D.; Luitz, J. *wien2k;* Technical Universität: Wien Austria, 2001.

(33) Schwarz, K.; Blaha, P. Solid state calculations using WIEN2k. *Comput. Mater. Sci.* **2003**, *28*, 259−273.

(34) Jones, R. O.; Gunnarsson, O. The density functional formalism, its applications and prospects. *Rev. Mod. Phys.* **1989**, *61*, 689.

(35) Perdew, J. P.; Burke, K.; Ernzerhof, M. Generalized gradient approximation made simple. *Phys. Rev. Lett.* **1996**, *77*, 3865.

(36) Petukhov, A.; Mazin, I.; Chioncel, L.; Lichtenstein, A. Correlated metals and the LDA+U method. *Phys. Rev. B: Condens. Matter Mater. Phys.* **2003**, *67*, 153106.

(37) Ravindran, P.; Fjellvåg, H.; Kjekshus, a.; Blaha, P.; Schwarz, K.; Luitz, J. Itinerant metamagnetism and possible spin transition in $LaCoO_3$ by temperature/hole doping. *J. Appl. Phys.* **2002**, *91*, 291−303.

(38) Blakely, C. K.; Bruno, S. R.; Poltavets, V. V. Low-temperature solvothermal approach to the synthesis of $La_4Ni_3O_8$ by topotactic oxygen deintercalation. *Inorg. Chem.* **2011**, *50*, 6696−6700.

(39) Wu, H. Charge−spin−orbital states in the tri-layered nickelate $La_4Ni_3O_8$: an *ab initio* study. *New J. Phys.* **2013**, *15*, 023038.

(40) Wells, A. F. *Structural Inorganic Chemistry;* Oxford University Press, 2012.

(41) Xiang, H.; Wei, S.-H.; Whangbo, M.-H. Origin of the structural and magnetic anomalies of the layered compound $SrFeO_2$: a density functional investigation. *Phys. Rev. Lett.* **2008**, *100*, 167207.

(42) Luque, A.; Martí, A. Increasing the efficiency of ideal solar cells by photon induced transitions at intermediate levels. *Phys. Rev. Lett.* **1997**, *78*, 5014.

(43) Okada, Y.; Sogabe, T.; Shoji, Y. *Advanced Concepts in Photovoltaics;* RSC Publishing, 2014; pp 425−454.

(44) Goodenough, J. *Magnetism and the Chemical Bond,* Interscience monographs on chemistry: Inorganic chemistry section; Interscience Publishers, 1963.

(45) Gopalakrishnan, J.; Colsmann, G.; Reuter, B. Studies on the $La_{2-x}Sr_xNiO_4$ ($0 \leq x \leq 1$) system. *J. Solid State Chem.* **1977**, *22*, 145−149.

(46) Takeda, Y.; Kanno, R.; Sakano, M.; Yamamoto, O.; Takano, M.; Bando, Y.; Akinaga, H.; Takita, K.; Goodenough, J. Crystal chemistry and physical properties of $La_{2-x}A_xNiO_4$ ($0 \leq x \leq 1.6$). *Mater. Res. Bull.* **1990**, *25*, 293−306.

(47) Munakata, F.; Takahashi, H.; Akimune, Y.; Shichi, Y.; Tanimura, M.; Inoue, Y.; Itti, R.; Koyama, Y. Electronic state and valence control of $LaCoO_3$: Difference between La-deficient and Sr-substituting effects. *Phys. Rev. B: Condens. Matter Mater. Phys.* **1997**, *56*, 979.

(48) Mackintosh, A. R.; McMorrow, D.; Jensen, J.; Ronnow, H. *Magnetism in Metals: A Symposium in Memory of Allan Mackintosh,* Copenhagen, 26−29 August 1996: Invited Review Papers; Kgl. Danske Videnskabernes Selskab, 1997; Vol. *45*.

DOI: 10.1021/acs.inorgchem.6b01938
Inorg. Chem. 2016, 55, 11898−11907